An Optimization of Wind Turbine Airfoil Possessing Good Stall Characteristics by Genetic Algorithm Utilizing CFD and Neural Network

Amir Latifi Bidarouni*‡, Mohammad Hasan Djavareshkian*

*Mechanical Engineering Department, Ferdowsi university of Mashhad

(a.latifi.b@gmail.com, javareshkian@ferdowsi.um.ac.ir)

‡Corresponding Author; Amir Latifi Bidarouni, Mechanical Engineering Department, Ferdowsi university of Mashhad, +98 511 880 5037, a.latifi.b@gmail.com

Received: 15.11.2013 Accepted: 09.12.2013

Abstract- In this research, an optimization of a wind turbine airfoil is performed by Genetic Algorithm (GA) as optimization method, coupled with CFD (Computational Fluid Dynamics) and Artificial Neural Network (ANN). A pressure-based implicit procedure is applied to solve the Navier-Stokes equations on a nonorthogonal mesh with collocated finite volume formulation to calculate the aerodynamic coefficients. The boundedness criteria for the numerical procedure are determined by Normalized Variable Diagram (NVD) scheme and the $k-\varepsilon$ eddy-viscosity turbulence model is utilized. ANN has been used as surrogate model to reduce computational cost and time. Single objective and multi objective optimization of wind turbine airfoil have been performed and the results of optimization are presented. To decrease the number of design variables and producing a smooth shaped airfoil, modified Hicks-Henne functions are applied. In this process, the Eppler E387 airfoil has been applied as the base airfoil. The angle of attack varies from 0 to 20 degrees and Reynolds number of the flow is 460000. The presented technique decreases the time of optimization by 99.5%. Moreover, the results manifest the good agreement of trained ANN outputs and CFD simulation. In addition, the Multi-objective optimization can attain the better solutions than single objective to design a wind turbine airfoil with good stall characteristics.

Keywords- Wind Turbine, ANN, GA, NVD, Optimization, Numerical Modeling.

1. Introduction

The Energy resources limitations and environmental concerns lead to an especial attention to optimization in engineering fields. Many airfoil optimizations have been performed in aerospace industries. Li et al. [1] have utilized an airfoil shape optimization method that reduces drag over a range of free stream Mach numbers. Buckley et al. [2] have optimized an airfoil in a range of on-design operating condition with the need to meet design constraints at various off-design operating conditions. Wickramasinghe et al. [3] illustrate the application of a reference point based many-objective particle swarm optimization algorithm to optimize low-speed airfoil aerodynamic design. Tashnizi et al. [4] have studied the effect of design variables vector on automatic aerodynamic shape optimization in the adjoint method. Hu et al. [5] address the aerodynamic performance of Busemann type supersonic bi-plane at off-design conditions. They have performed an adjoint based optimization technique to optimize the aerodynamic shape of the biplane to reduce the wave drag. Mohamad et al. [6] concentrate on the optimization of a symmetric airfoil shape leading to the best possible performance of a monoplane wells turbine with constant solidity. Silisteanu and Botez [7] present a fast method to design two-dimensional airfoils in which the design process starts from an already known airfoil or from a new defined airfoil by imposing some basic geometrical characteristics such as: leading edge radius or trailing edge slope.

Climate change and air pollution have forced scientists to look for other sources of sustainable and clean energies. Today, wind energy is the most economical kind of

renewable energy and research in wind turbine increased in the recent years. Winnemöller and Van Dam [8] have optimized a thick airfoil and their optimization objectives are the maximization of both moment of inertia and lift to drag ratio. Mauclèr [9] offers a method for the design of wind turbine airfoils based on direct numerical optimization of a B-spline representation of the airfoil shape. The XFOIL is applied as flow solver during the optimization. Thumthae and Chitsomboon [10] have performed the numerical simulation of horizontal axis wind turbines (HAWTs) with untwisted blade to determine the optimal angle of attack that produces the highest power output. Singh et al. Endo [11] has optimized a two-dimensional shape of wind turbine by means of Particle Swarm Optimization. He utilizes Re-Normalized Group (RNG) $k-\varepsilon$ model to calculate flow field around airfoil. Bizzarrini et al. [12] have designed an airfoil by genetic algorithm coupled with RFOIL for tip region of wind turbine blade. [13] have designed a low Reynolds airfoil based on existing low Reynolds number airfoils for small wind turbines. They have performed it by altering the leading edge noise radius, airfoil thickness and trailing edge thickness of existing airfoils independently and comparing the Cl and Cl/Cd of new airfoils. Richard Vesel Jr. [14] have optimized a 5 MW wind turbine rotor blade based on the NREL 5 MW reference wind turbine to maximize efficiency and minimum flapwise hub heading moment. Singh and Ahmed [15] present the design and performance results of a small horizontal axis wind turbine rated at 400 W with a 1.26 m diameter, 2-bladed rotor designed for low Re applications in the wind speed range of 3 to 6 m/s.

Gradient Based optimization (GB) method is recommended for linear optimization problems, because of its fast convergence to the answer. Aerodynamic problems are multimodal and GB may stick in local minima. Hence, Evolutionary Algorithms (EA) must be utilized. EAs require performing lots of iterations. When the problem is complex, for instance, in aerodynamic optimization, EAs will be very time consuming and possessing high computational cost, because each complete analysis last long. One method to overcome this disadvantage of EAs is using of surrogate models. Alexandrov et al. [16] have studied an approach, first-order approximation and model management optimization for solving design optimization problems that involve computationally expensive simulations. Kusiak et al. [17] present a multi-objective optimization of wind turbine performance and ANN has been applied to capture dynamic equations to model wind turbine performance. Kusiak et al. [18] have presented a data-driven approach for the maximization of the power by wind turbines. The power optimization objective is accomplished by computing optimal control settings of wind turbines using applying data mining and evolutionary strategy algorithms. Kusiak and Zheng [19] integrate data mining and evolutionary computation to optimize the power factor and the amount of power produced by a wind turbine. Riberio et al. [20] have coupled GA with CFD and ANN as a surrogate model to design a wind turbine airfoil in high angles of attack. A complete optimization process in their work consists of several CFD simulations and an ANN training. In addition, objective function is the same for entire process. They have decreased computational cost by 50%. Djavareshkian and Esmaeili [21] have optimized an hydrofoil applying an Adaptive Neuro-Fuzzy Inference System (ANFIS) model to predict the hydrofoil performance.

The objective of this research is the optimization of wind turbine airfoil at design angle of attack where lift to drag ratio is at the highest value and possessing a good stall characteristic. In the initial process, GA is coupled with a pressure-based implicit procedure to solve the Navier-Stokes equations on a nonorthogonal mesh with collocated finite volume formulation for the calculation of the aerodynamic coefficients. In the numerical method, the boundedness criteria for the numerical procedure are determined by Normalized Variable Diagram (NVD) scheme and the $k-\varepsilon$ eddy-viscosity turbulence model is utilized. Then, in the training process of ANN, the results of numerical simulation are used to train the neural network. A method is described to predict the aerodynamic coefficients of an airfoil with ANN. The accuracy of predicted aerodynamic coefficients by ANN is distinguished. Finally, GA and trained ANN are utilized to obtain the optimum airfoil geometry for wind turbines. This technique is very fast in respect to traditional optimization methods. It can decrease the computational cost by 99.5%. It is confirmed that ANN is very powerful, reliable and applicable algorithm to predict the aerodynamic coefficients.

2. Governing Equation and Discretization

The basic equations which describe the conservation of mass, momentum and scalar quantities can be expressed in the following vector forms which are independent in the coordinate system.

$$\frac{\delta\rho}{\delta t}+div\left(\rho\vec{V}\right)=S_m \tag{1}$$

$$\frac{\delta(\rho\vec{V})}{\delta t}+div\left(\rho\vec{V}\otimes\vec{V}-\vec{T}\right)=\vec{S}_v \tag{2}$$

$$\frac{\delta(\rho\phi)}{\delta t}+div\left(\rho\vec{V}\phi-\vec{q}\right)=\vec{S}_\phi \tag{3}$$

The last two equations are usually expressed in terms of basic dependent variables. The stress tensor for a Newtonian fluid is:

$$\vec{T}=-P\vec{I} \tag{4}$$

and the Fourier-type law usually gives the scalar flux vector:

$$\vec{q}=\Gamma_\phi grad\phi \tag{5}$$

In this study, $k-\varepsilon$ model is utilized for turbulence flow. The $k-\varepsilon$ model is simple and has good stability with easy convergence. The discretization of the above differential equations is carried out by using a finite-volume approach. First, the solution domain is divided into a finite number of

discrete volumes or cells, where all variables are stored at their geometric centers (see e.g. Fig. 1).

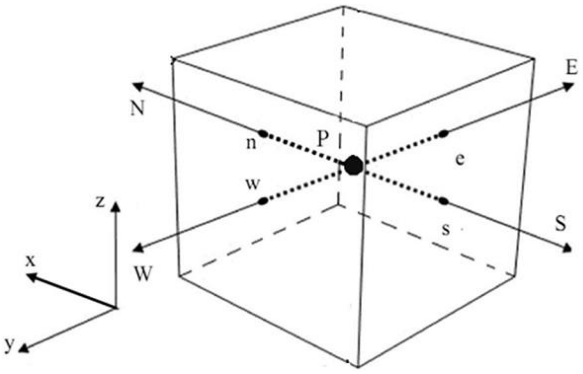

Fig. 1. Finite volume and storage arrangement.

The equations are then integrated over all the control volumes by utilizing the Gaussian theorem. The discrete expressions are presented to refer to only one face of the control volume, namely, e, for the sake of brevity. For any variable ϕ (which may also stand for the velocity components), the result of the integration yields:

$$\frac{\delta v}{\delta t}\left[(\rho\phi)_p^{n+1}-(\rho\phi)_p^{n}\right]+I_e-I_w+I_n-I_s=S_\phi\delta v \qquad (6)$$

Where $I's$ are the combined cell-face convection I^C and diffusion I^D fluxes. The diffusion flux is approximated by central differences. The discretization of the convective flux requires special attention and it causes to develop the various schemes. A representation of the convective flux for cell-face (e) is:

$$I_e^C=(\rho.V.A)_e\,\phi_e=F_e\phi_e \qquad (7)$$

The value of ϕ_e is not known and it should be estimated from the values at neighboring grid points by interpolation. The expression for the ϕ_e is determined by the SBIC scheme [22], that is based on the NVD technique [23] using interpolation from the nodes E, P and W. The functional relationship utilized in SBIC scheme for $\bar{\phi}_e$ is presented as:

$$\begin{aligned}
&\bar{\phi}_e=\bar{\phi}_p, && IF\ \bar{\phi}_p\notin[0,1]\\
&\bar{\phi}_e=-\frac{\bar{x}_p-\bar{x}_e}{\mathcal{K}(\bar{x}_p-1)}\bar{\phi}_p^{\,2}+\left(1+\frac{\bar{x}_p-\bar{x}_e}{\mathcal{K}(\bar{x}_p-1)}\right)\bar{\phi}_p, && IF\ \bar{\phi}_p\in[0,\mathcal{K}]\\
&\bar{\phi}_e=\frac{\bar{x}_p-\bar{x}_e}{\bar{x}_p-1}+\frac{\bar{x}_p-\bar{x}_e}{\bar{x}_p-1}\bar{\phi}_p, && IF\ \bar{\phi}_p\in[\mathcal{K},1]
\end{aligned} \qquad (8)$$

Where

$$\bar{\phi}_p=\frac{\phi_p-\phi_W}{\phi_E-\phi_W}, \qquad \bar{\phi}_e=\frac{\phi_e-\phi_W}{\phi_E-\phi_W}$$

$$\bar{x}_p=\frac{x_p-x_W}{x_E-x_W}, \qquad \bar{\phi}_e=\frac{x_e-x_W}{x_E-x_W} \qquad (9)$$

The limits on the selection of $\mathcal{K}$ could be determined by the following ways. Obviously, the lower limit is $\mathcal{K}=0$ which would represent switching between upwind and central difference. It is not favorable, because it is essential to avoid the abrupt switching between the schemes in order to achieve the converged solution. The value of $\mathcal{K}$ should be kept as low as possible in order to attain the maximum resolution of the scheme. The final form of the discretized equation from each approximation is given as:

$$a_p.\phi_p=\sum_{m=E,W,N,S}a_m.\phi_m+S_\phi^{'}+S_{dc} \qquad (10)$$

Where, $a's$ are the convection-diffusion coefficients . The term $S_\phi^{'}$ in Eq. 10 contains quantities arising from non-orthogonality, numerical dissipation terms and external sources. For the momentum equations, it is easy to separate out the pressure-gradient source from the convection momentum fluxes. S_{dc} is the contribution due to the adapted deferred correction procedure.

3. Boundary Condition

At the inlet of the domain, velocities are prescribed and the pressure is obtained by zero order extrapolation from interior points. At outlet, the pressure is fixed. The far-field boundary is set to 30c from the airfoil to minimize its undesired effects on the flow surrounding and is set to slip boundary conditions. The non-slip condition is applied at the airfoil surfaces. To account for the steep variations in turbulent boundary layers near solid walls, wall functions which define the velocity profile in the vicinity of no-slip boundaries are employed.

Gradient Based Algorithms (GB) supposedly will fall in local minima in aerodynamic problems, because aerodynamic phenomena are multimodal. Overcoming this problem, EAs are recommended and utilized in these cases. Thus, Genetic Algorithm (GA) which is an EA is applied in this research. GA is a stochastic optimization method to find the minimum or maximum of a problem as the best solution. The principles of genetics and natural selection is the basis of GA [24].

At first, in this algorithm an initial population which is composed of specific number of individuals generates. Then, at each generation, GA performs operations such as selection, elitism, crossover and mutation to let the population evolve and maximize the particular fitness. In one hand, selection and elitism increase the chance of producing the individuals with higher fitness in the next generations and in the other hand, mutation and crossover make GA to search the domain randomly for probable optimum solutions.

4. Geometry Generation

Reducing the number of design variables is essential in global optimization, because each design variable will add some complexity to the problem and this will increase the time of optimization process, considerably. There are several ways to produce a smooth shaped airfoil with just a few numbers of variables instead of working with lots of numbers of the airfoil's coordinate points. To approach this purpose, Hicks-Henne functions have been applied in this work. The geometry of new airfoil can be obtained with Eq. 11 [25].

$$y_{new} = y_{base} + \sum_{i=1}^{n} \alpha_i f_i \tag{11}$$

Where y_{new} is the y coordinate of new airfoil, y_{base} is the y coordinate of base airfoil which in this research, Eppler E387 airfoil coordinate has been selected. α_i, $\left(i = 1, 2, .., 16\right)$ are design variables. Eight design variables have been considered for upper side of airfoil $\left(\alpha_1 \, to \, \alpha_8\right)$ and other eight design variables have been looked upon for lower side of airfoil $\left(\alpha_9 \, to \, \alpha_{16}\right)$. This means that there are sixteen design variables totally which will be generated by GA at each generation. f_i $\left(i = 1, 2, .., 8\right)$ are shape functions and should be calculated from Eqs. 12 to14.

$$f_k\left(x\right) = \sin\left(\pi\left(1-x\right)^{e(k)}\right) \quad \text{,k=1,2} \tag{12}$$

$$f_k\left(x\right) = \sin^3\left(\pi x^{e(k)}\right) \quad \text{,k=3,4,5} \tag{13}$$

$$f_k\left(x\right) = \sin\left(\pi x^{e(k)}\right) \quad \text{,k=6,7,8} \tag{14}$$

Where x is the coordinate of airfoil related to y_{base} or y_{new}, k is the number of design variables on each side of airfoil and $e\left(k\right)$ can be calculated from Eqs. 15 and 16.

$$e\left(k\right) = \ln 0.5 / \ln\left(1 - x_k\right) \quad \text{k=1,2} \tag{15}$$

$$e\left(k\right) = \ln 0.5 / \ln\left(x_k\right) \quad \text{k=3,4,5,6,7,8} \tag{16}$$

Where x_k, $\left(k = 1, 2, \ldots, 8\right)$ determines where maximum of f_k occurs and is sundry from x. values for x_k which have been applied in this work are illustrated in Table 1.

Table 1. The values of which have been used

x_1	x_2	x_3	x_4	x_5	x_6	x_7	x_8
0.08	0.15	0.20	0.30	0.45	0.60	0.75	0.92

It's prominent to note that each of design variables must be bounded to a certain range, because GA can just search in a region that has been assigned to it. The wider region increases the chance of finding a better solution, but it will take more time. Accordingly, the range which assigned to each design variable should be determined somehow to possess a good compromise between gaining a better solution and time. However, by using ANN which reduces the time of optimization, a wide region is selected in this article to ensure that the best solutions are obtained. The upper and lower bounds of each design variables are attained after several trial and errors and the final results are illustrated in Table 2. Shadowed area in Fig. 2 illustrates the domain where Genetic Algorithm searches to find the optimum solution.

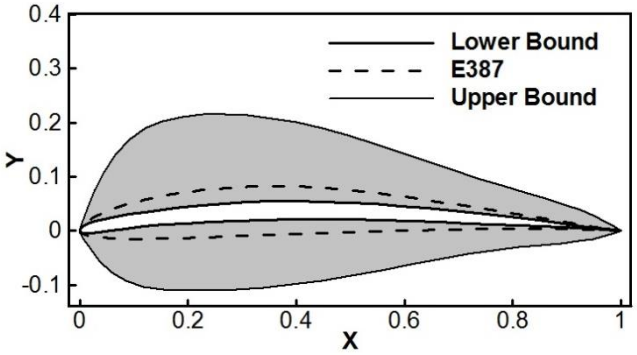

Fig. 2. The illustration of domain where Genetic Algorithm searches

Table 2. The upper and lower bounds for each design variables

Design variables	Lower bound	Upper bound
α_1	-0.0055	0.04
α_2	-0.006	0.04
α_3	-0.007	0.04
α_4	-0.009	0.03
α_5	-0.008	0.03
α_6	-0.005	0.02
α_7	-0.002	0.02
α_8	-0.00001	0.01
α_9	-0.0055	0.03
α_{10}	-0.006	0.02
α_{11}	-0.007	0.03
α_{12}	-0.009	0.02
α_{13}	-0.008	0.03
α_{14}	-0.005	0.02
α_{15}	-0.002	0.01
α_{16}	-0.00001	0.01

5. Artificial Neural Network (ANN)

Artificial Neural Network (ANN) is a simple model of biological neurons. Neural networks are good in fitting functions to any set of practical data. It consists of inputs, layers and outputs. Each layer includes the weight matrix **W**,

the summers, the bias vector **b**, the transfer function *tf* and the output vector **t**. Each layer's input which multiplied by weight matrix sums in summer with bias vector which has been multiplied with 1 and the result leads to transfer function. A network without bias vectors has zero output for zero input and this is not desirable, moreover bias makes the network more powerful [26] that's why bias vectors are utilized here. Network architecture that is used in this research is illustrated in Fig. 3. This is a feed forward network with 3 layers.

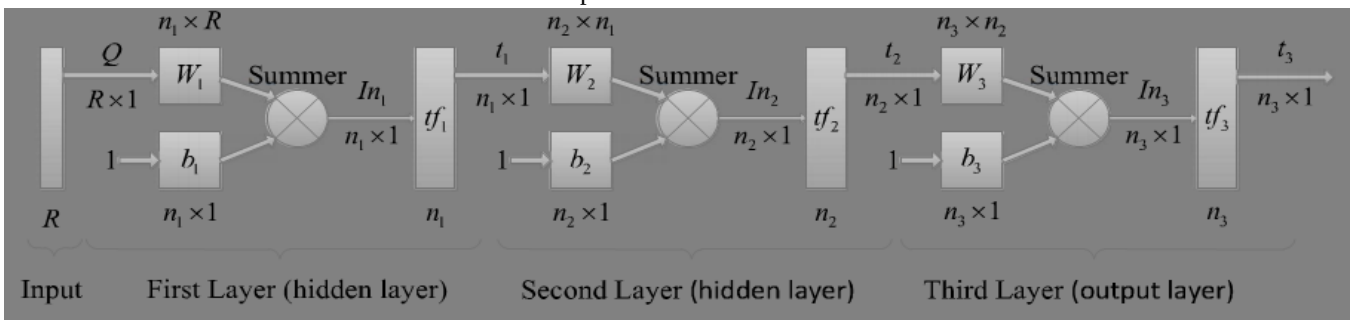

Fig. 3. The architecture of Artificial network used[26].

Q is the network's input vector and R is the size of that. The input of ANN are design variables which are sixteen plus an angle of attack which means that there is seventeen independent variables, totally as ANN's input. Table 3 manifests a sample data as ANN's input for one random airfoil. This is a small part of entire input data. It is notable that for any airfoil, all rows are the same and just seventeenth column which the angle of attack is changed. n_i is the number of neurons in i-th layer, tf_i is the transfer function of i-th layer and In_i is the input of tf_i. The size of each element is written below or above it in Fig. 3. The row number of the weight matrix **W** indicates the number of neurons in its layer while the column number of that is the number of layer's input. The layer whose output is the entire network's output is output layer (third layer) and the two others are hidden layers. For hidden layers, the output of transfer function is the input of next layer[26].

Table 3. The sample of data as Neural Network's input

α_1	α_2	...	α_{15}	α_{16}	*AOA*
0.027996	0.00272	...	0.007363	0.002982	0
0.027996	0.00272	...	0.007363	0.002982	6
. . .	. . .	...	. . .	. . .	. . .
0.027996	0.00272	...	0.007363	0.002982	18
0.027996	0.00272	...	0.007363	0.002982	20

The output of network can be calculated from Eq. 17.

$$a_3 = tf_3\left(W_3 tf_2\left(W_2 tf_1\left(W_1 q + b_1\right) + b_2\right) + b_3\right) \qquad (17)$$

R is equal to the number of problem's input. The number of neurons for the output layer n_3 is equal to the number of problem's output. It is desirable that ANN predicts the values of lift, drag and moment coefficients about one fourth of chord from leading edge related to each set of Network's input. Therefore, here, the number of output is three. Table 4 shows sample data as ANN's target and related to those data in Table 3. In an ideal trained neural network, the outputs of ANN must be equal to the targets.

Table 4. The sample of data as ANN's target and related to those data in Table 3

C_l	C_d	$C_{m_{c/4}}$
0.225871	0.038546	-0.0422
0.77316	0.054639	-0.04163
. . .	. . .	. . .
1.162999	0.198523	-0.04913
1.071324	0.23491	-0.05597

There is no certain method to determine the other parameters of network architecture. These parameters which are the number of layers and the number of neurons in each one must be determined by try and error. Here, several networks with various network architecture i.e. sundry numbers of layers and different numbers of neurons in each layer have been examined to define the appropriate network architecture. For all examined networks, transfer function of hidden layers is Hyperbolic Tangent Sigmoid and transfer function for output layer is linear. The Levenberg-Marquardt learning algorithm is applied, because the network is relatively small and this algorithm is fast and efficient for this kind of networks [27] and also it is proper for the purpose of function fitting [26]. The Mean Square Error (MSE) is selected as ANN's performance. Training algorithm adjust weights in a way to minimize the MSE.

6. Methodology

In the process of optimization, GA generates a population of design variables. Each individual in this population consists of sixteen design variables $\left(\alpha_1 \text{ to } \alpha_{16}\right)$ within the aforementioned bounds of Table 2 to produce a new airfoil. Each unique set of these variables create a particular airfoil. Hicks-Henne function utilizes these parameters to calculate the new airfoil coordinates. Then, suitable mesh will be created for this newly introduced airfoil. The Navier-Stokes equations are solved to simulate the flow around it at nine various angles of attack to predict the aerodynamic coefficients. These angles are presented in Table 5.

Table 5. The angles of attack

AOA_1	AOA_2	AOA_3	AOA_4	AOA_5	AOA_6	AOA_7	AOA_8	AOA_9
0	6	8	10	12	14	16	18	20

The results of numerical simulation are used to train sundry ANN architecture when sixty airfoil shapes have been analyzed. When several ANN architectures are examined, then the network architecture with lower MSE is elected as trained ANN. The flow chart applied in this paper for ANN training illustrated in Fig. 4.

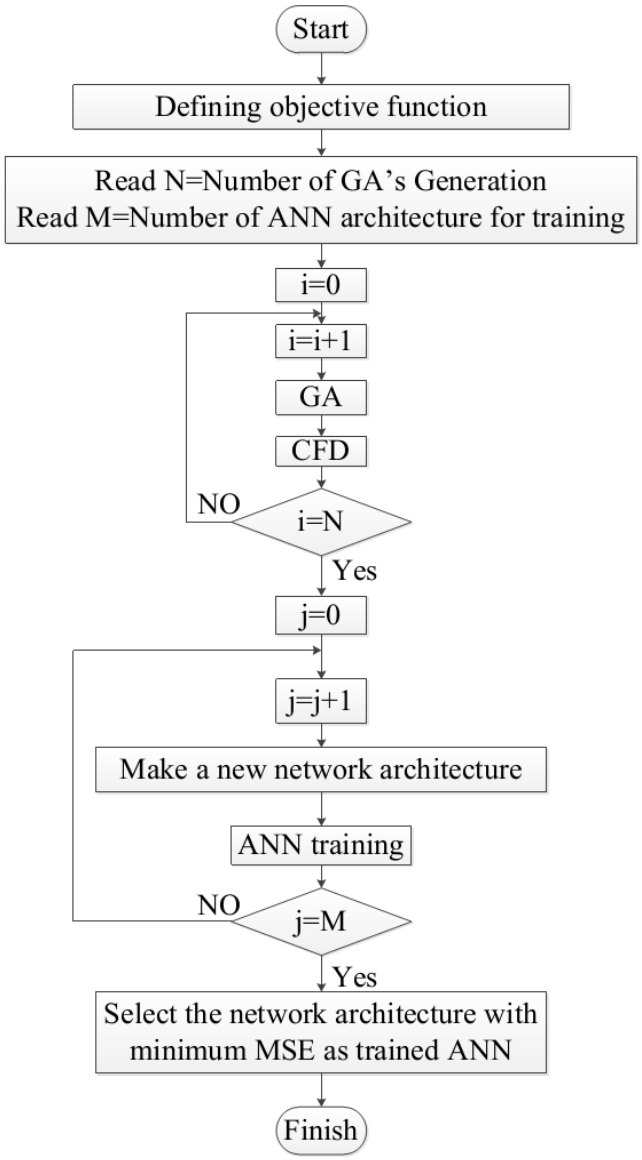

Fig. 4. The flow chart utilized to train ANN

Then the trained ANN have been applied for the rest optimization processes with any desirable objective function. Flow chart of optimization with GA and trained ANN demonstrated in Fig. 5.

In the present research, the training process is separated from optimization procedure. Therefore, any optimization with any objective function can be performed with this trained ANN. There is no need to carry out more CFD simulation for new optimizations. This technique leads to a significant reduction in computational cost.

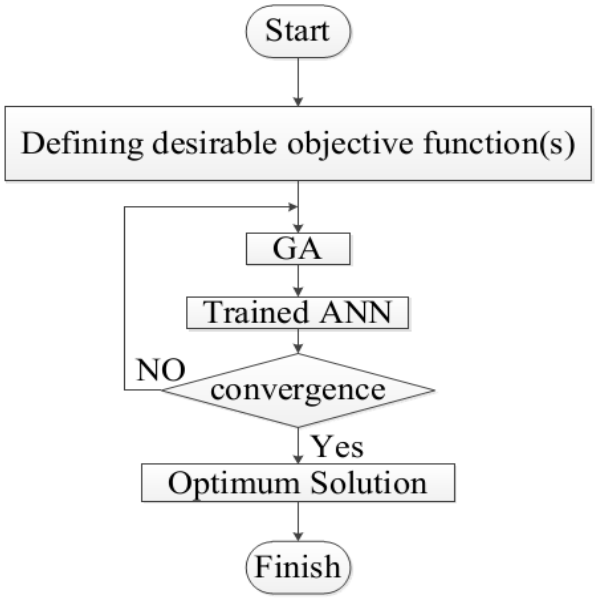

Fig. 5. The flow chart to optimize with GA and ANN

7. Objective Functions

Sometimes, the local angle of attack for wind turbines becomes very high, because the wind direction is not the same for all the times or for high angular velocity of rotor blade due to high wind speed. Thus, it is eminent to design an airfoil not only with good performance in design angle of attack where lift to drag ratio is maximum [28], but also to possess a good stall characteristic [29],[30]. Hence, the objective functions which are considered here are the mentioned parameters.

8. Results and Discussion

In the numerical simulation, the result must be independent of grid and domain. Also, numerical procedure and results must be validated by comparing them with experiment and published data. The grid structure that is used in CFD simulation is created by a structured mesh, because of its simplicity and applicability to the current problem. The two dimensional structured grid which is applied in this research illustrated in Fig. 6. The domain and grid sizing is determined by doing several different trials. For instance, the effect of grid size is demonstrated in Fig. 7. According to this figure, to simulate the flow a mesh with 26650 numbers of nodes is utilized. In Fig. 8, the pressure distribution on the surface of NACA0012 with zero angle of attack at Reynolds number equal to 6×10^6 is indicated and validated with experimental data [31]. These comparisons prove that the numerical results are in a good agreement with experimental data.

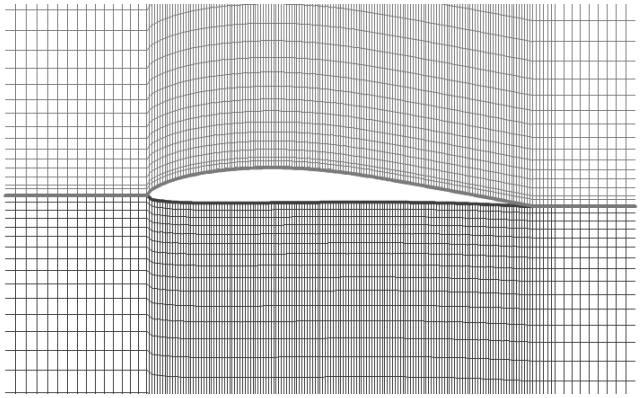

Fig. 6. The part of the H Grid

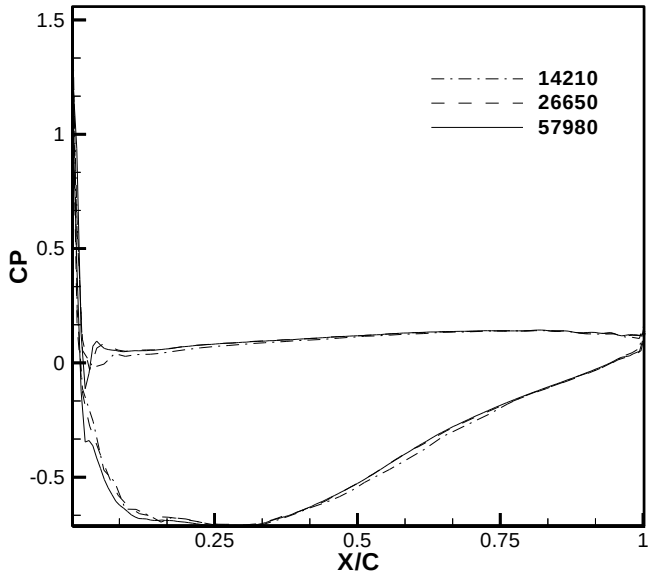

Fig. 7. The effect of grid sizing on pressure distribution on the surface of the E387 airfoil for an angle of attack 1.6˚

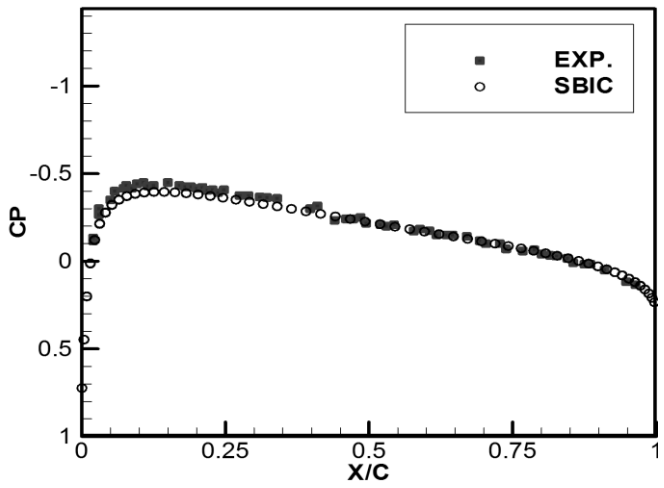

Fig. 8. The comparison of numerical and experimental pressure coefficient distribution around airfoil NACA0012 with $\alpha = 0^{\circ}$

As mentioned before, MSE is selected as ANN's performance. In other words, MSE is a measure to distinguish the ability of a network in predicting the targets. In Fig. 9, the performance of several examined networks architecture are illustrated. Horizontal axis of this figure is the network architecture, for example, 8-8-3 means 8 neurons in first layer, 8 neurons in second layer and 3 neurons in output layer. Here, 8-8-3 is the best, because not only it has the lowest MSE, but also manifests no significant overfitting or underfitting and performance value is approximately equal for training, test, and validation sets.

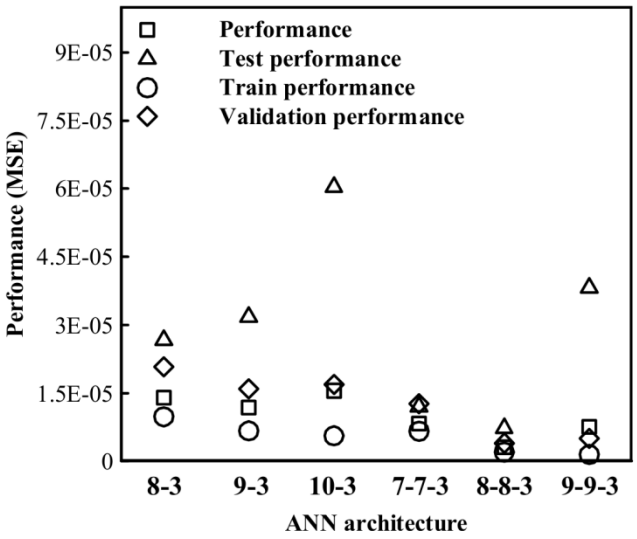

Fig. 9. The performance of several networks architecture

The regression plot of this network's outputs with respect to targets is demonstrated in Fig. 10. It is important to note that in a perfect fitting, data must lie in 45 degree line i.e. the line whose outputs of the network is equal to targets $\left(Output = Target\right)$. This figure indicates that suitable weights are calculated and ANN is able to predict the aerodynamic coefficients, accurately. It can be concluded from these two figures that 8-8-3 Network is eligible to use as surrogate model. Therefore it is used for all optimizations which have been performed in this research.

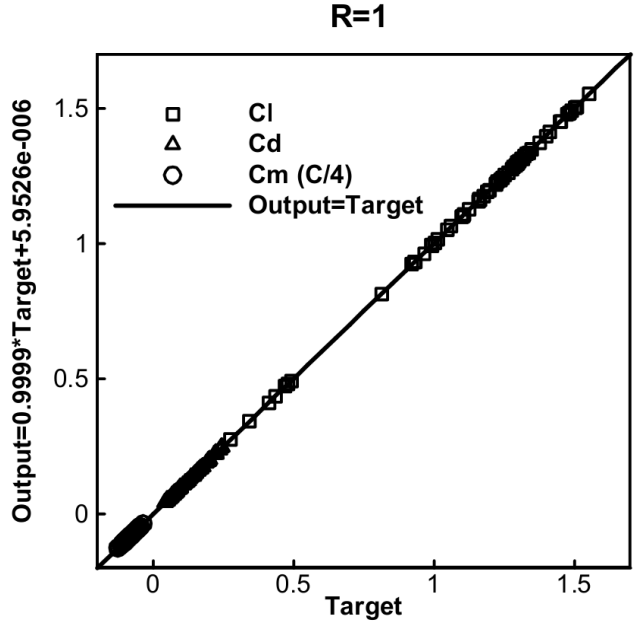

Fig. 10. The regression plot of 8-8-3 network's outputs with respect to targets.

Two single objective optimizations and one multi-objective optimization have been performed. Objective functions are as follows:

Single objective optimization case (1): Maximizing Lift to drag ratio at $AOA = 6°$

Single objective optimization case (2): Maximizing maximum lift coefficients.

Multi-objective optimization case (3): Maximizing both Lift to drag ratio at $AOA = 6°$ and maximum lift coefficient, simultaneously.

The comparison of lift coefficient for optimized airfoils and base airfoil is illustrated in Fig. 11. It indicates that all optimized airfoils have higher lift coefficients than base airfoil. Furthermore, multi-objective optimization not only finds an airfoil with higher lift coefficient respect to case 1, but also attains an airfoil whose stall takes place at higher angle of attack. This means that the latter one has better stall characteristics than the former. With regard to these explanations and this figure, case 2 has the best stall characteristics.

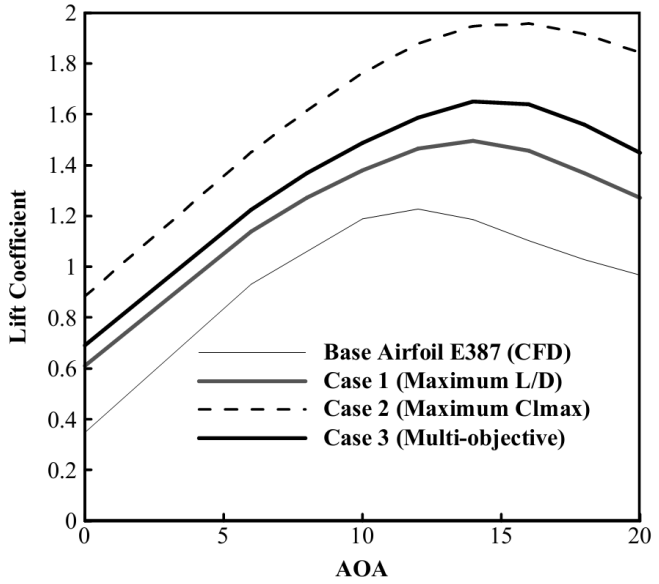

Fig. 11. The lift coefficient comparison of optimized airfoils with base airfoil

The percentage of improvement in Lift to drag ratio for optimized airfoils is illustrated in Fig. 12. This percentage is calculated from Eq. 18.

$$improvement = \left(L/D_O - L/D_B\right)/\left(L/D_B\right)\times 100 \quad (18)$$

Where L/D_O and L/D_B are lift to drag ratio of optimized airfoil and base airfoil, respectively, which the last one is obtained from CFD.

This figure confirms that cases 1 and 3 improve airfoils performance not only in lower angles of attack where wind turbine usually works, but also in the higher angles of attack. This proves that these two optimizations are better than case 2. The results of cases 1 and 3 demonstrate that their performance are the same at the angles of attack close to six, but their various results can be observed at the other angles. The last two figures illustrate that case 3 with the mentioned objective functions has the best airfoil with good performance improvement and stall characteristics.

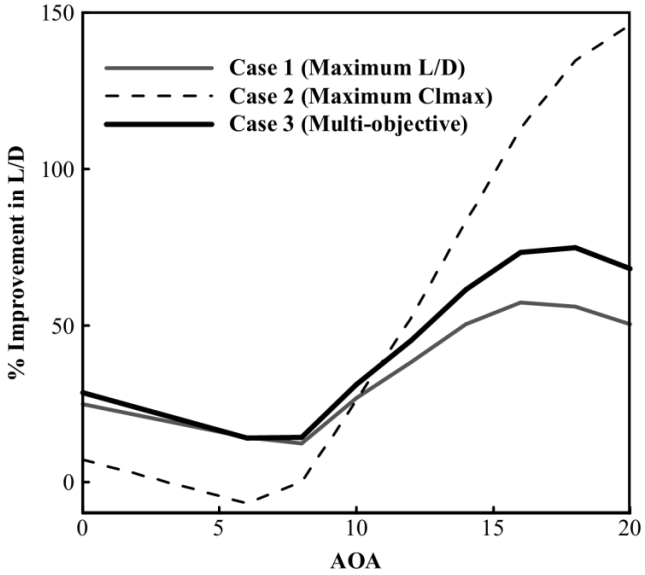

Fig. 12. The percentage of improvement in lift to drag ratio of optimized airfoils respect to base airfoil from CFD.

The shape of optimized airfoils and base airfoil are illustrated in Fig. 13. It indicates that cases 3 and 1 have the same shape, approximately, and it could be anticipated from Fig. 12 because their improvement in lift to drag ratio are nearly alike. For lower side, all optimized airfoils are near the lower bound, this implies that search domain in lower side of airfoil can be decreased. For upper side and for case 1, the search domain can be decreased, but for case 2, the search domain must be as wider as possible. This means that if the objective function is selected as a maximizing lift to drag ratio, smaller search domain is necessitated, because the optimized airfoil tends to be thinner. But, if the objective function is defined as a maximizing lift coefficient, the wider region is required, because optimized airfoil tends to be thicker.

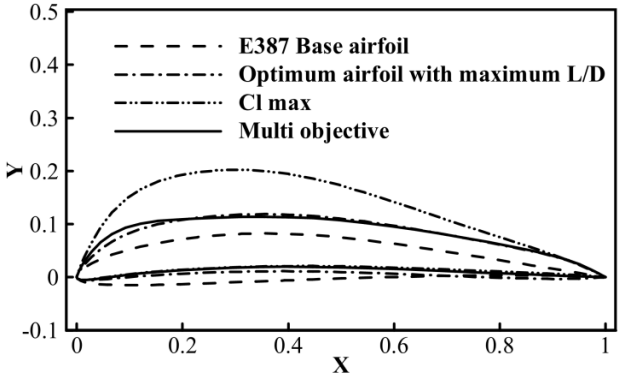

Fig. 13. The comparison of optimized airfoils and base airfoil E387

The amount of time which is saved with this method is calculated with Eq. 19 and is reported in Table 6.

$$t_s = \left(n_o - n_t\right)/n_o \times 100 \quad (19)$$

Where t_s is the percentage of time which is saved by this method and n_o and n_t are number of generations in entire optimization process and in training process, respectively. It assumes that the time of optimization with ANN is negligible respect to CFD analysis. In this research n_t is equal to 3.

Table 6. The percentage of time saved in this method

n_o	50	100	200	400	600	800	900	1000
Cl_{max}	1.8675	1.8714	1.9023	1.9209	1.9526	1.9566	1.9584	1.9590
t_s	94%	97%	98.5%	99.25%	99.5%	99.625%	99.667%	99.7%

It can be concluded from this table that Cl_{max} is approximately constant after 600 generations. Consequently, this method can yield 99.5% saving in time in respect to the state that all the optimization process performed with CFD.

The lift coefficient of optimized airfoil in respect to the angle of attack by CFD and ANN for case 3 is illustrated in Fig. 14. This comparison confirms that ANN can predict the aerodynamic coefficients the same as CFD analysis and approves this optimization.

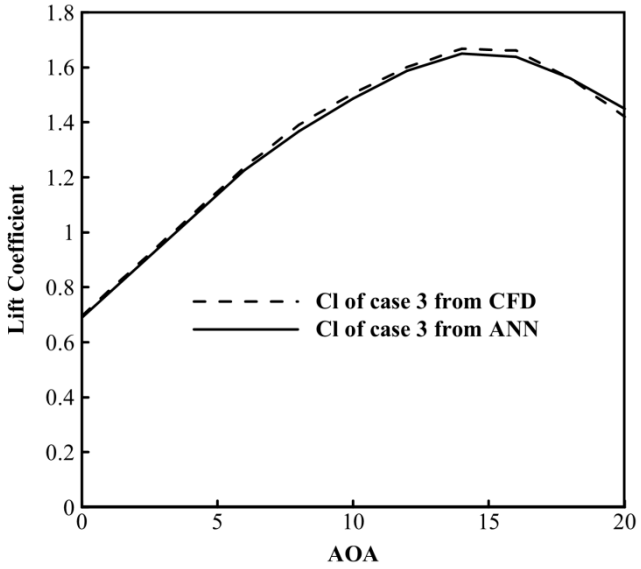

Fig. 14. The lift coefficient of optimized airfoil case 3 obtained with both ANN and CFD analysis

9. Conclusion

In this research, a pressure-based implicit procedure to solve the Navier-Stokes equations on a nonorthogonal mesh with collocated finite volume formulation is utilized for the calculation of the aerodynamic coefficients. The genetic algorithm with Artificial Neural Network are applied to attain an optimization of wind turbine airfoil with good stall characteristics. The main points of the achievements in this essay are:

1) The presented technique decreases the time of optimization by 99.5%.
2) The agreement between presented numerical results by utilizing high resolution scheme and experimental data is considerable.
3) The outputs of trained ANN and the results that obtained from CFD simulation are coincident.
4) The multi-objective optimization can attain the better solutions than single objective to design a wind turbine airfoil with good stall characteristics.
5) To optimize a wind turbine airfoil, it is better to select the upper side region larger than lower side region.

The improvement in airfoil's performance attained by this technique at design angle of attack is approximately 15%.

Nomenclature

GA	=	Genetic Algorithm	Γ	=	Diffusivity Coefficient
NVD	=	Normalized Variable Diagram	I^c	=	Convection Flux
CFD	=	Computational Fluid Dynamic	I^D	=	Diffusion Flux
k	=	Turbulence Model Parameter	δv	=	Cell Volume
ε	=	Turbulence Model Parameter	F	=	Mass Flux
$\vec{S}$	=	Source Term	A	=	Cell Face Area
T	=	Time	$\bar{x}$	=	Normalized Coordinate
CL	=	Lift Coefficient	$\mathcal{K}$	=	SBIC Parameter
CD	=	Drag Coefficient	A	=	convection-diffusion coefficient
c	=	Cord Length	P	=	Pressure
AOA	=	Angle of Attack	ANN	=	Artificial Neural Network
ρ	=	Density	μ	=	Dynamic Viscosity
$\vec{V}$	=	Velocity Vector	N	=	Iteration Number
$\vec{T}$	=	Stress Tensor	M	=	Iteration Number
ϕ	=	Scalar Quantity	dv	=	Displacement due to new Velocity
$\vec{q}$	=	Scalar Flux Vector	Re	=	Reynolds Number
$SBIC$	=	Second and Blending Interpolation Combined	$SIMPLE$	=	Semi-Implicit Method For Pressure – Linked Equation

$S_{\phi}^{'}$	=	Source Term from non-orthogonality, numerical dissipation terms and external sources

References

[1] W. Li, L. Huyse, and S. Padula, "Robust airfoil optimization to achieve drag reduction over a range of Mach numbers," Structural and Multidisciplinary Optimization, vol. 24, pp. 38-50, 2002/08/01 2002.

[2] B. Howard, Z. Beckett, and Z. David, "Airfoil Optimization Using Practical Aerodynamic Design Requirements," in 27th AIAA Applied Aerodynamics Conference, ed: American Institute of Aeronautics and Astronautics, 2009.

[3] U. K. Wickramasinghe, R. Carrese, and L. Xiaodong, "Designing airfoils using a reference point based evolutionary many-objective particle swarm optimization algorithm," in Evolutionary Computation (CEC), 2010 IEEE Congress on, 2010, pp. 1-8.

[4] E. S. Tashnizi, A. A. Taheri, and M. H. Hekmat, "Investigation of the adjoint method in aerodynamic optimization using various shape parameterization techniques," Journal of the Brazilian Society of Mechanical Sciences and Engineering, vol. 32, pp. 176-186, 2010.

[5] H. Rui, J. Antony, and W. Qiqi, "Adjoint based aerodynamic optimization of supersonic biplane airfoils," in 49th AIAA Aerospace Sciences Meeting including the New Horizons Forum and Aerospace Exposition, ed: American Institute of Aeronautics and Astronautics, 2011.

[6] M. H. Mohamed, G. Janiga, E. Pap, and D. Thévenin, "Multi-objective optimization of the airfoil shape of Wells turbine used for wave energy conversion," Energy, vol. 36, pp. 438-446, 2011.

[7] S. Paul and B. Ruxandra, "Two-dimensional airfoil shape optimization for airfoils at low speeds," in AIAA Modeling and Simulation Technologies Conference, ed: American Institute of Aeronautics and Astronautics, 2012.

[8] T. Winnemöller and C. P. Van Dam, "Design and Numerical Optimization of Thick Airfoils Including Blunt Trailing Edges," Journal of Aircraft, vol. 44, pp. 232-240, 2007/01/01 2007.

[9] X. Mauclère, "Automatic 2D Airfoil Generation, Evaluation and Optimisation using MATLAB and XFOIL," Master of science, Mechanical Engineering Department section of fluid mechanics, Technical University of Denemark, 2009.

[10] C. Thumthae and T. Chitsomboon, "Optimal angle of attack for untwisted blade wind turbine," Renewable Energy, vol. 34, pp. 1279-1284, 5// 2009.

[11] M. Endo, "Wind Turbine Airfoil Optimization by Particle Swarm Method," Case Western Reserve University, 2011.

[12] N. Bizzarrini, F. Grasso, and D. P. Coiro, "Genetic algorithms in wind turbine airfoil design," presented at the EWEA, Brussels, Belgium, 2011.

[13] R. K. Singh, M. R. Ahmed, M. A. Zullah, and Y.-H. Lee, "Design of a low Reynolds number airfoil for small horizontal axis wind turbines," Renewable Energy, vol. 42, pp. 66-76, 6// 2012.

[14] R. W. V. Jr, "Aero-Structural Optimization of a 5 MW Wind Turbine Rotor," Degree Master of Science, Mechanical and Aerospace Engineering, The Ohio State University, 2012.

[15] R. K. Singh and M. R. Ahmed, "Blade design and performance testing of a small wind turbine rotor for low wind speed applications," Renewable Energy, vol. 50, pp. 812-819, 2// 2013.

[16] N. Alexandrov, R. Lewis, C. Gumbert, L. Green, and P. Newman, "Approximation and Model Management in Aerodynamic Optimization with Variable-Fidelity Models," Journal of Aircraft, vol. 38, pp. 1093-1101, 11/01/ 2001.

[17] A. Kusiak, Z. Zijun, and L. Mingyang, "Optimization of Wind Turbine Performance With Data-Driven Models," Sustainable Energy, IEEE Transactions on, vol. 1, pp. 66-76, 2010.

[18] A. Kusiak, H. Zheng, and Z. Song, "Power optimization of wind turbines with data mining and evolutionary computation," Renewable Energy, vol. 35, pp. 695-702, 3// 2010.

[19] A. Kusiak and H. Zheng, "Optimization of wind turbine energy and power factor with an evolutionary computation algorithm," Energy, vol. 35, pp. 1324-1332, 3// 2010.

[20] A. F. P. Ribeiro, A. M. Awruch, and H. M. Gomes, "An airfoil optimization technique for wind turbines," Applied Mathematical Modelling, vol. 36, pp. 4898-4907, 10// 2012.

[21] M. H. Djavareshkian and A. Esmaeili, "Neuro-fuzzy based approach for estimation of Hydrofoil performance," Ocean Engineering, vol. 59, pp. 1-8, 2013.

[22] M. Djavareshkian, "A new NVD scheme in pressure-based finite-volume methods," 2001, pp. 10-14.

[23] B. P. Leonard, "A survey of finite differences with upwinding for numerical modeling of the incompressible convection diffusion equation in C. Taylor and K. Morgan leds " Technices in Transient and Turbulent Flow, Pineridgequess, Swansea, U.K., vol. 2, pp. 1-35, 1981.

[24] R. L. Haupt and S. E. Haupt, "Introduction to Optimization," in Practical Genetic Algorithms, ed: John Wiley & Sons, Inc., 2004, pp. 1-25.

[25] R. M. Hicks and P. A. Henne, "Wing Design by Numerical Optimization," Journal of Aircraft, vol. 15, pp. 407-412, 1978/07/01 1978.

[26] M. T. Hagan, H. B. Demuth, and M. Beale, Neural network design: PWS Publishing Co., 1996.

[27] Y. Hao and M. W. Bogdan, "Levenberg?Marquardt Training," in Intelligent Systems, ed: CRC Press, 2011, pp. 1-16.

[28] E. Hau, Wind Turbines: Fundamentals, Technologies, Application, Economics: Springer, 2006.

[29] M. O. L. Hansen, Aerodynamics of wind turbines [electronic resource]: Earthscan, 2008.

[30] G. Francesco, "Hybrid Optimization for Wind Turbine Thick Airfoils," in 53rd AIAA/ASME/ASCE/AHS/ASC Structures, Structural Dynamics and Materials Conference, ed: American Institute of Aeronautics and Astronautics, 2012.

[31] "Experimental data base for computer program assessment," tech.rep.,AGARD Advisory Report No. 138.